J. Fluid Mech. (1984), *vol.* 149, *pp.* 33–58
Printed in Great Britain

Hydrodynamics and heat transfer associated with condensation on a moving drop: solutions for intermediate Reynolds numbers

By T. SUNDARARAJAN AND P. S. AYYASWAMY
University of Pennsylvania, Philadelphia, PA 19104

(Received 17 October 1983 and in revised form 19 June 1984)

The hydrodynamics and heat/mass transport associated with condensation on a moving drop have been investigated for the intermediate Reynolds-number range of drop motion ($Re = O(100)$). The drop environment is a mixture of saturated vapour and a non-condensable. The formulation entails a simultaneous solution of the quasi-steady elliptic partial differential equations that describe the flow field and transport in the gaseous phase, and the motion inside the liquid drop. The heat transport inside the drop is treated as a transient process. Results are reported for the interfacial velocities, drag, external and internal flow structure, heat flux, drop growth rate and temperature–time history inside the drop. The results obtained here have been compared with experimental data where available, and these show excellent agreement.

The results reveal several novel features. The surface-shear stress increases with condensation. The pressure level in the rear of the drop is higher. As a consequence, the friction drag is higher and the pressure drag is lower. The total drag coefficient increases with condensation rate for small values of drop size or temperature differential, and it decreases for large values of these parameters. The volume of the separated-flow region in the rear of the drop decreases with condensation. At very high rates of condensation, the recirculatory wake is completely suppressed. Condensation also delays the appearance of the weak secondary internal vortex motion in the drop. The heat and mass fluxes are significantly affected by the presence of the non-condensable in the gaseous phase and by the circulation inside the drop.

1. Introduction

Condensation on moving drops occurs in a wide variety of physical situations. For instance, condensation on a spray of drops is encountered in various studies on raindrops, in the design of an emergency cooling spray system in a nuclear-reactor containment, etc. However, the condensation phenomenon on translating drops has not been examined in sufficient detail. In particular, the effects of condensation on drop motion and on drag phenomena do not seem to have been investigated. The intent of the present paper is to analyse the hydrodynamics and the transport phenomena associated with condensation on a single moving drop, for a wide range of condensation rates. Although realistic situations demand the consideration of a spectrum of moving drops of various sizes, there is still a great need for a fundamental understanding of the single-drop problem.

There are many studies in the literature that involve heat and mass transfer and/or hydrodynamics of drop motion (Clift, Grace & Weber 1978). Specifically, with regard

to condensation on drops, Nix & Fukuta (1972), Lou & Yang (1979) and Rakhmatulina (1981) have studied stationary drops. Ford & Lekic (1973) have experimentally investigated the growth rate of a water drop in a pure steam environment. Kulic, Rhodes & Sullivan (1975) and Kulic & Rhodes (1978) have predicted condensation heat-transfer rates for droplets moving in air–steam mixtures using standard heat-transfer correlations. They have also experimentally recorded the temperature–time history of a water drop experiencing condensation in a forced flow of steam and air (Kulic & Rhodes 1977). Sadhal & Ayyaswamy (1983) and Chung, Ayyaswamy & Sadhal (1984*a*, *b*) have theoretically examined slowly moving drops. Condensation in the vicinity of the front stagnation point of a drop in high-Reynolds-number motion has been investigated by Chung & Ayyaswamy (1981*a*, *b*). A boundary-layer formulation appropriate for intermediate Reynolds numbers has been provided by Sundararajan & Ayyaswamy (1984*a*).

In this paper we examine condensation on a spherical drop that is translating with a flow Reynolds number $Re = O(100)$. The drop environment is a saturated mixture of condensable vapour and a non-condensable gas. Condensation on the entire drop surface has been considered. The flow problems inside and outside the drop have been simultaneously treated. A constant-property quasi-steady model describes the transport in the gaseous phase. The quasi-steady flow solutions and transport rates to the drop are obtained in terms of the instantaneous values of two non-dimensional parameters (one, Re, representing the flow conditions, and the other, W, representing the thermodynamic conditions). The elliptic partial differential equations for the gaseous phase are solved by a hybrid finite-difference scheme. The scheme involves central-differencing near the drop surface and upwind-differencing in the far field. It provides accurate results near the drop while guaranteeing numerical stability in the far field. The drop heating is treated as a transient process in view of the relatively slow diffusion of heat in the liquid phase. The heat equation is suitably formulated in terms of a stream-function coordinate and is solved by the Crank–Nicolson procedure. The more general transient treatment of the drop interior (both the flow and heat-up) is the subject of a separate investigation (Sundararajan & Ayyaswamy 1984*b*).

Although the formulations developed here are suitable for application to many liquid–vapour systems in the presence of non-condensables, only results appropriate for the water–steam system with air as the non-condensable have been studied.

2. Physical description

Consider the introduction of a cold water drop of radius R into an environment consisting of a mixture of vapour (steam) and non-condensable (air). The total pressure p_∞ and temperature T_∞ of the saturated mixture are taken to be prescribed. The drop is colder than its environment and condensation occurs on the drop surface. The shear stress at the interface due to drop translation will initiate liquid circulation inside the drop. The heat deposited on the drop surface will heat the drop liquid. For a short period of time following the introduction of the drop, rapid transients in velocity, temperature and concentration will occur in both the liquid and gaseous phases.

Let the instantaneous translational velocity of the drop be U_∞. For a particle in the gaseous phase, the typical residence time adjacent to the drop surface is $O(R/U_\infty)$. On the other hand, for a particle in the liquid phase, the typical residence time is $O(R/U_s)$, where U_s is the maximum circulation velocity at the drop surface. Since

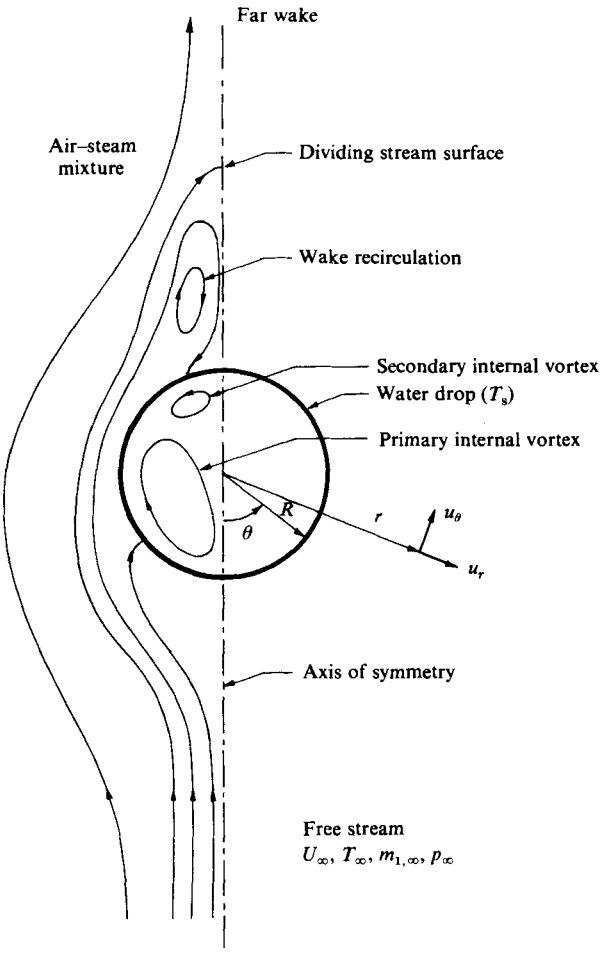

FIGURE 1. Geometry of the problem.

the rapid transients arise due to the sudden contact between the two phases, the residence-time estimates provided above are the characteristic times for the rapid transient processes. For a circulating water drop translating in a gas–vapour mixture, U_s/U_∞ may be shown to be $O(10^{-1})$ or less. Therefore it may be inferred that the period during which rapid transients occur is $O(R/U_s)$ and corresponds to a few circulation cycles inside the drop. Subsequent to this initial period of rapid transients, changes in flow and transport take place at a much slower rate until the drop thermally equilibrates with the outside. This latter period, during which the bulk of the condensation occurs, is the subject-matter of the present study.

We consider a coordinate frame that coincides with the drop centre and moves with the instantaneous bulk velocity U_∞ of the drop (figure 1). The Reynolds number of translation (hereinafter referred as Re_g) is taken to be $O(100)$, but less than, say, 500. For $Re_g \gtrsim 500$ flow instabilities such as drop oscillations and vortex shedding are known to occur. The flow may not be laminar and the deformation from the spherical shape of the drop may be large (Clift *et al.* 1978). In our analysis the drop deformation due both to inertial effects (Weber number We) and to hydrostatic-pressure variation (Eötvös number Eo) are assumed to be small. We consider water drops of size 1 mm diameter or less ($Eo < 0.4$ and $We < 0.3$). Next consider the circulation inside the

drop. From a shear-stress balance across the liquid–gas interface it may be estimated that $U_s/U_\infty = O[(\rho_g\mu_g/\rho_\ell\mu_\ell)^{\frac{1}{2}}]$ for $Re_g = O(10^2)$ (Law, Prakash & Sirignano 1977). Also, $Re_\ell/Re_g = O[(\mu_g^2\rho_\ell/\mu_\ell^2\rho_g)^{\frac{2}{3}}]$, where Re_ℓ is the circulation Reynolds number based on U_s. For the range of Re_g considered in the present study, it may be noted that Re_ℓ is also $O(10^2)$. Therefore the flow pattern inside the drop resembles a Hill's spherical vortex (Batchelor 1956). Since the liquid Prandtl number Pr_ℓ is $O(10)$, the Péclet number Pe_ℓ for heat transport inside the drop is $O(10^3)$.

Condensation causes a radially inward flow towards the drop surface. The non-zero mass flux at the interface alters the translational flow field and modifies the drag on the drop. Also, the radial flow leads to a build-up of the non-condensable concentration near the drop-surface above that in the far stream. The accumulation results in a mass-transfer resistance and a consequent reduction in the transport rates.

For $Re_g = O(10^2)$ flow separates on the rear of the drop. A recirculatory wake is formed, whose dimensions in the absence of condensation may be comparable to the drop size (Clift *et al.* 1978). The radial flow due to condensation reduces the wake size. In our analysis, the effects of non-condensable accumulation, liquid circulation and external-flow separation are taken into account.

3. Quasi-steady analysis

Beyond the initial period of rapid transients, the transport to the drop surface may be regarded as quasi-steady. The quasi-steady behaviour may be demonstrated by comparing the timescales of the various convective and diffusive processes in both the phases.

In the gaseous phase (except in the far wake), the residence time R/U_∞ of a typical fluid particle near the drop surface determines the timescales for convection and diffusion of momentum, energy and species. For the liquid phase, however, a distinction must be made between the quantities in the streamwise and the cross-stream directions. In the streamwise direction the timescale for convection of both heat and momentum is R/U_s. The streamwise diffusion may be ignored in view of $Re_\ell = O(10^2)$. For the cross-stream direction, where only diffusion effects are present, the timescales for the transport of momentum and heat are R^2/ν_ℓ and R^2/α_ℓ respectively. Here ν_ℓ and α_ℓ are the appropriate diffusivities. The comparison of the various timescales in the increasing order is

gas-phase flow and transport	: convection of momentum and heat in the streamwise direction in liquid	: diffusion of momentum in cross-stream direction in liquid	: diffusion of heat in cross-stream direction in liquid

$$\equiv \frac{R}{U_\infty} : \frac{R}{U_s} : \frac{R^2}{\nu_\ell} : \frac{R^2}{\alpha_\ell}.$$

Setting $R^2/\alpha_\ell = 1$, in the scale of the drop heat-up, the above timescales become

$$\frac{U_s}{U_\infty}\frac{1}{Pe_\ell} : \frac{1}{Pe_\ell} : \frac{1}{Pr_\ell} : 1.$$

For $U_s/U_\infty = O(10^{-1})$, $Pe_\ell = O(10^3)$ these are

$$10^{-4} : 10^{-3} : 10^{-1} : 1.$$

It is obvious that, in the timescale of the drop heating, all other processes may be regarded as quasi-steady. This observation enables a great simplification in the mathematical structure of the problem.

Apart from the quasi-steady approximation, certain assumptions are made in the analysis. These are as follows. (i) Surface tension is large and constant on the interface. (ii) Both the liquid and the vapour–gas mixture are pure systems. Surfactants that alter interfacial tension or inhibit condensation by offering interfacial resistance are assumed to be absent. (iii) the liquid–vapour interface is at the thermodynamic equilibrium; and non-equilibrium effects due to condensation are negligible. The partial pressure of the vapour at the interface is equal to the vapour pressure corresponding to the drop-surface temperature. The gas–vapour mixture behaves like an ideal-gas mixture. The finite condensation rate does not alter the vapour pressure. (iv) Property variations with temperature and non-condensable concentration are not included, for the sake of simplicity. (v) The instantaneous surface temperature T_s of the drop is taken to be uniform over the drop surface. For dimensionless times greater than $O(Pe_\ell^{-1})$ this assumption may be justified for high Pe_ℓ (see Appendix A). The uniform-surface-temperature assumption is useful in decoupling the quasi-steady equations from the formulation for the drop heat-up (Harpole 1981). (vi) In the liquid phase the stream surfaces are taken to be isothermal. As already demonstrated, the timescale of heat convection in the liquid (streamwise direction) is $O(Pe_\ell^{-1})$ compared with the timescale of cross-stream heat diffusion. Thermal effects propagate very much faster in the streamwise direction relative to those in the cross-stream direction. A faster equalization of temperature occurs in the streamwise direction. (vii) Viscous-dissipation, compressibility effects are ignored. (viii) Radiative heat transport has been neglected, although gas-phase convective heat transport has been retained for completeness. For the parameters of our study, both the convective and radiative heat transports are very small in the presence of condensation. However, for the temperature levels encountered in our study, the convective heat transport is an order of magnitude larger than the radiative contribution. We note that, for extremely small rates of condensation, the gas-phase convective heat-transport contribution may become significant.

The non-dimensional quasi-steady equations are as follows:

for the gaseous phase (subscript g refers to the mixture, 1 to the non-condensable, 2 to vapour)

$$\nabla\cdot\boldsymbol{u}_g = 0, \tag{1}$$

$$\boldsymbol{u}_g\cdot\nabla\boldsymbol{u}_g = -\tfrac{1}{2}\nabla p_g + \frac{2}{Re_g}\nabla^2\boldsymbol{u}_g, \tag{2}$$

$$\boldsymbol{u}_g\cdot\nabla T_g = \frac{2}{Pe_{g,t}}\nabla^2 T_g, \tag{3}$$

$$\boldsymbol{u}_g\cdot\nabla w_1 = \frac{2}{Pe_{g,m}}\nabla^2 w_1; \tag{4}$$

for the liquid phase (subscript ℓ refers to the liquid phase)

$$\nabla\cdot\boldsymbol{u}_\ell = 0, \tag{5}$$

$$\boldsymbol{u}_\ell\cdot\nabla\boldsymbol{u}_\ell = -\tfrac{1}{2}\nabla p_\ell + \frac{2}{Re_\ell}\nabla^2\boldsymbol{u}_\ell. \tag{6}$$

In the above, $\boldsymbol{u}_g$ *is the mass average velocity for the binary mixture of air and water vapour.*

The velocities $\boldsymbol{u}_g$ and $\boldsymbol{u}_\ell$ have been scaled by U_∞; pressures p_g and p_ℓ are $(p_g^*-p_\infty)/\frac{1}{2}\rho_g U_\infty^2$ and $(p_\ell^*-p_\infty)/\frac{1}{2}\rho_\ell U_\infty^2$; ρ is density; temperature T_g is equal to $(T_g^*-T_\infty)/(T_s-T_\infty)$, while the normalized mass fraction w_1 is $(m_1-m_{1,\infty})/(m_{1,s}-m_{1,\infty})$. The starred quantities are dimensional. m_1 is the mass fraction of the non-condensable. Also,

$$Re_g = \frac{U_\infty 2R}{\nu_g}, \quad Re_\ell = \frac{U_\infty 2R}{\nu_\ell}, \quad Pe_{g,t} = \frac{U_\infty 2R}{\alpha_g}, \quad Pe_{g,m} = \frac{U_\infty 2R}{D_{12}},$$

where ν, α and D are the kinematic viscosity, thermal diffusivity and mass diffusivity. Pe is the Péclet number. The boundary conditions are as follows.

At the interface $(r = 1)$

Continuity of tangential velocity:

$$u_{g,\theta} = u_{\ell,\theta} = u_\theta. \tag{7a}$$

Continuity of shear stress:

$$r\frac{\partial}{\partial r}\left(\frac{u_{g,\theta}}{r}\right)+\frac{1}{r}\frac{\partial u_{g,r}}{\partial\theta} = \frac{\mu_\ell}{\mu_g}\left[r\frac{\partial}{\partial r}\left(\frac{u_{\ell,\theta}}{r}\right)+\frac{1}{r}\frac{\partial u_{\ell,r}}{\partial\theta}\right]. \tag{7b}$$

Continuity of mass flux across the interface:

$$\rho_g(u_{g,r}-\dot{R}) = \rho_\ell(u_{\ell,r}-\dot{R}), \tag{7c}$$

where $\dot{R}$ is the growth rate of the drop. In the context of the spherical-shape assumption it is valid to consider a uniform growth of the drop for all angles, and $\dot{R}$ is then given by

$$\rho_g(\bar{u}_{g,r}-\dot{R}) = -\rho_\ell\dot{R},$$

where $\bar{u}_{g,r}$ is the average gas-phase radial velocity at the interface. The normal velocity on the liquid side of the moving interface is therefore

$$\rho_g(u_{g,r}-\bar{u}_{g,r}) = \rho_\ell u_{\ell,r}.$$

However, in view of $Re_\ell = O(10^2)$ and $\rho_\ell/\rho_g = O(10^3)$, $u_{\ell,r}$ can be set equal to zero for the estimation of the liquid flow without much loss of accuracy. Thus

$$u_{\ell,r} = 0. \tag{7d}$$

The equation for normal stress balance need not be considered in view of the large surface tension and the assumed spherical shape of the drop.

The interface is impermeable to the non-condensable species. The convective and diffusive fluxes of the non-condensable balance each other at the interface at each instant of time. The condensation velocity at the interface may therefore be written as

$$\frac{2W}{Pe_{g,m}}\frac{\partial w_1}{\partial r} = \hat{u}_c = \frac{u_c}{Pe_{g,m}}, \tag{7e}$$

where $\hat{u}_c$ and u_c are the non-dimensional condensation velocities given by $\hat{u}_c = u_c^*/U_\infty$ and $u_c = u_c^*/(D_{12}/2R)$. The parameter W, referred to as the condensation parameter, is given by $W = 1-m_{1,\infty}/m_{1,s}$, and it is a function of the thermodynamic conditions p_∞, T_∞ and T_s. W varies from 0 to 1. The limit zero corresponds to a non-condensing situation and $W = 1$ to a pure-vapour environment.

Temperature continuity:

$$T_g = T_\ell = 1. \tag{7f}$$

Heat continuity:

$$Ja_g \frac{\partial T_g}{\partial r} + \frac{1}{2Le_g}\left[u_c + \frac{\rho_g \bar{u}_c}{\rho_\ell - \rho_g}\right] = q_s, \tag{7g}$$

where the Jakob number Ja_g is given by $Ja_g = c_{pg}(T_\infty - T_s)/\lambda$, $Le_g = \alpha_g/D_{12}$ is the Lewis number for the gaseous phase, and the non-dimensional heat flux is given by $q_s = q_s^* R/\rho_g \alpha_g \lambda$. The latent heat of condensation is λ, and the specific heat is c_p. The term $\rho_g \bar{u}_c/(\rho_\ell - \rho_g)$ arises owing to drop growth, and $\bar{u}_c$ is the average value of u_c. The normalized mass fraction at the interface:

$$w_1 = 1. \tag{7h}$$

Far-stream conditions $(r \to \infty)$

Uniform velocity:

$$\boldsymbol{u}_g = -\boldsymbol{i}, \tag{7i}$$

where $\boldsymbol{i}$ is the unit vector along the axis for $\theta = 0$. The bulk mixture conditions are

$$T_g = p_g = w_1 = 0. \tag{7j}$$

Axisymmetric conditions at $\theta = 0$ *and* $\theta = \pi$

$$u_{g,\theta} = \frac{\partial u_{g,r}}{\partial \theta} = \frac{\partial p_g}{\partial \theta} = \frac{\partial T_g}{\partial \theta} = \frac{\partial w_1}{\partial \theta} = 0, \tag{7k}$$

$$u_{\ell,\theta} = \frac{\partial u_{\ell,r}}{\partial \theta} = \frac{\partial p_\ell}{\partial \theta} = 0. \tag{7l}$$

In the numerical computations, the following values (typical for condensation of steam in the presence of air) have been used: $Pr_g = 0.85$, $Sc = 0.6$, $\mu_\ell/\mu_g = 40$ and $\rho_\ell/\rho_g = 1000$. The quasi-steady condensation process is studied for several combinations of Re_g and W. Correlations are then developed for the heat flux and the drag.

4. Transient drop heating

The correlations for heat flux and drag are coupled with the heat transport inside the drop, and the transient evolution of drop heating is evaluated. The energy equation for the liquid phase is

$$\frac{\partial T_\ell}{\partial t} + \tfrac{1}{2} Pe_\ell [\boldsymbol{u}_\ell \cdot \nabla T_\ell] = \nabla^2 T_\ell. \tag{8}$$

Here the temperature T_ℓ has been non-dimensionalized as

$$T_\ell = \frac{T_\ell^* - T_0}{T_\infty - T_0}, \quad t = \int \frac{\alpha_\ell \, dt^*}{R^2}, \quad Pe_\ell = \frac{U_\infty 2R}{\alpha_\ell}.$$

T_0 is the initial bulk temperature of the drop. Since the stream surfaces inside the drop are isothermal, the energy equation (8) may be suitably recast in terms of the stream-function coordinate based on the Hill's spherical vortex. This facilitates the numerical solution.

Following Kronig & Brink (1950) and Brignell (1975), we employ a normalized stream-function coordinate m and an orthogonal streamwise coordinate ξ, which are given by

$$m = 4r^2(1-r^2)\sin^2\theta, \quad \xi = \frac{r^4\cos^4\theta}{2r^2-1}. \tag{9}$$

The metric coefficients h_m, h_ξ and h_ϕ in the (m, ξ, ϕ)-coordinate system are

$$h_m = \frac{1}{8r\Delta\sin\theta}, \quad h_\xi = \frac{(2r^2-1)^2}{4r^3\Delta\cos^3\theta}, \quad h_\phi = r\sin\theta, \tag{10}$$

where $\Delta^2 = (1-2r^2)^2\sin^2\theta + (1-r^2)^2\cos^2\theta$. Defining the streamwise-average liquid temperature $\bar{T}_\ell$ as

$$\bar{T}_\ell = \frac{\oint T_\ell h_m h_\xi h_\phi \,\mathrm{d}\xi}{\oint h_m h_\xi h_\phi \,\mathrm{d}\xi}, \tag{11}$$

where the cyclical integral is over a closed stream surface, the energy equation (8) may be written in the form

$$H(m)\frac{\partial \bar{T}_\ell}{\partial t} = \frac{\partial}{\partial m}\left[J(m)\frac{\partial \bar{T}_\ell}{\partial m}\right], \tag{12}$$

where

$$H(m) = -\frac{1}{2}\oint h_m h_\xi h_\phi \,\mathrm{d}\xi, \quad J(m) = -\frac{1}{2}\oint \frac{h_\xi h_\phi}{h_m}\mathrm{d}\xi.$$

The liquid phase boundary conditions are as follows. At the drop surface ($m = 0$), continuity of heat flux gives

$$(q_s^*)_{av} = -\frac{k_\ell(T_\infty - T_0)}{R}\frac{\partial T_\ell}{\partial r}\bigg|_{av} = \frac{16}{3}\frac{k_\ell(T_\infty - T_0)}{R}\frac{\partial \bar{T}_\ell}{\partial m}\bigg|_0, \tag{13a}$$

At the centre of the vortex ($m = 1$), $\bar{T}_\ell$ and its derivatives should be finite. This leads to

$$\frac{\partial \bar{T}_\ell}{\partial t} = \frac{1}{H(m)}\frac{\partial J}{\partial m}\frac{\partial \bar{T}_\ell}{\partial m}\bigg|_1. \tag{13b}$$

The initial condition is

$$\bar{T}_\ell = 0 \quad \text{at} \quad t = 0. \tag{14}$$

The transient heat-up of the drop interior may now be evaluated by solving this initial-value problem.

5. Numerical procedure

5.1. *Evaluation of the gaseous-phase transport*

The governing equations (1)–(6) and boundary conditions (7*a–l*) are transformed in terms of the dimensionless stream function ψ (scaled with $U_\infty R^2$) and vorticity ζ (scaled with U_∞/R). In spherical coordinates (figure 1) the stream function and vorticity are

$$\boldsymbol{u}_g = \boldsymbol{\nabla}\times\left\{-\frac{\psi_g}{r\sin\theta}\boldsymbol{e}_\phi\right\}, \quad \zeta_g\boldsymbol{e}_\phi = \boldsymbol{\nabla}\times\boldsymbol{u}_g, \tag{15}$$

where $\boldsymbol{e}_\phi$ is the unit vector in the ϕ-direction. Similar expressions apply for the liquid side.

Owing to the elliptic nature of the governing equations, the far-stream boundary conditions, and the location of their specification, significantly influence the numerical solutions. Here the far-stream conditions are specified on a large but finite spherical surface of radius R_∞. The value of R_∞ needs to be judiciously chosen as a compromise between the computational effort and the desired accuracy for the solutions. Some important considerations for selecting a proper value of R_∞ are (i) the asymptotic approach to the far-stream conditions of uniform velocity, temperature, and concentration; (ii) the magnitude of the radial velocity induced by the condensation at R_∞; and (iii) the volume of the separated-flow region behind the drop. The radius R_∞ must be large enough so that the uniform stream conditions are essentially realized there; and the strength of the radial flow at R_∞ due to the condensation should be very small compared with that due to translation. The solution domain defined by R_∞ must enclose the drop, the gaseous boundary layers and the recirculatory wake region. We employ limiting solutions corresponding to potential flow and pure radial flow to check for the uniformity in conditions and for the strength of the condensation-induced radial flow. Estimates for wake sizes in the absence of radial flow are available (Clift *et al.* 1978), and these are used as preliminary, conservative guesses in deciding the value of R_∞. A considerable amount of numerical experimentation is necessary before an appropriate choice is finally made.

The solution domain is divided into a grid with a variable step size. A fine spacing is employed near the drop, where the gradients are steep. A coarse spacing is adequate in the far stream, where the gradients are weak. An exponential grid spacing is generated by making a transformation $r = e^z$, and considering equal spacing in z. A constant angular step size is used for the θ-coordinate. Typically $\Delta z = 0.025$, $\Delta\theta = 3°$, and a grid with 91×61 exterior nodes and 41×61 interior nodes have been used. Also, R_∞ is typically ten times the drop radius in the calculations (see figure 2).

To predict the transport to the drop accurately, a central-difference scheme (CDS) with a second-order accuracy is employed near the drop. But CDS has not been used throughout the solution domain for the sake of computational economy. In a convection-dominated situation, central-differencing of the convective derivative (gradient that is multiplied by velocity) causes numerical oscillations unless the grid size is very small (Spalding 1972; Joseph 1983). To use CDS throughout would have therefore required very small step sizes even in the far field. To circumvent this difficulty, an upwind-difference scheme (UDS) is used far away from the drop. The UDS does not have cell-size restrictions for numerical stability (Patankar 1980). It must be recognized that, at intermediate Reynolds numbers, numerical stability may not imply convergence of the solution (Joseph 1983), and careful numerical experimentation is necessary before reliable solutions are obtained. The UDS is also known to suffer from 'artificial diffusion' (Vahl Davis & Mallinson 1976) and 'false scaling' (Strikwerda 1982), and cannot provide sufficiently accurate results near the drop. The scheme used in the present paper is modelled after the one proposed by Spalding (1972) and Runchal (1972), incorporating recommendations made in later publications (Gupta 1973; Raithby 1976). In the hybrid scheme, at the start of every iteration, based on the current-guess solutions, the coefficients for the convective and diffusive terms are estimated at each grid point using CDS. The CDS is retained where the coefficient for the diffusion contribution is larger, and the UDS is employed when the coefficient for convection becomes dominant.

The nonlinear algebraic difference equations are solved iteratively, starting from suitable guess solutions. A successive over-relaxation procedure is used to accelerate the convergence. Computations are carried out until the changes in the predicted

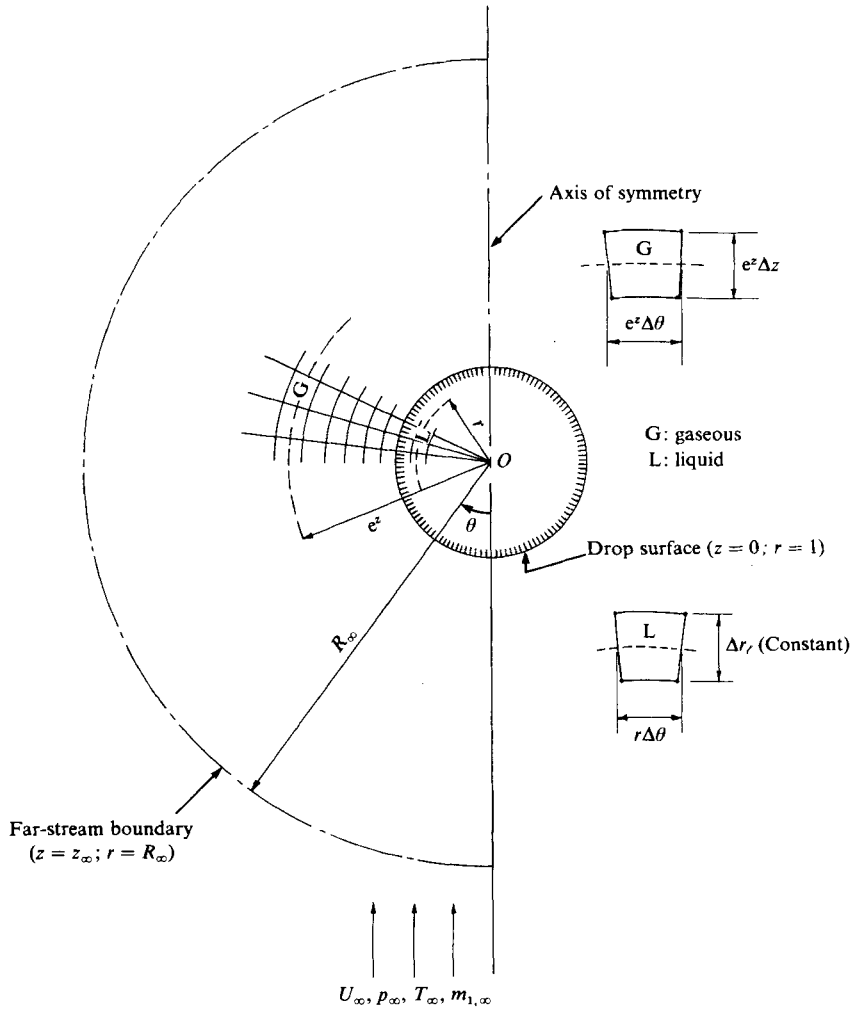

FIGURE 2. The coordinate grids inside and outside the drop.

transport quantities are less than 10^{-7} (absolute error) or less than 0.1 % (relative error) between successive iterations. The time for a typical computer run, involving one combination of Re_g and W, is of the order of 60 minutes on the Univac 1100/62 computer.

5.2. *Evaluation of drop heat-up*

A Crank–Nicolson procedure is used to evaluate the transient heat-up of the drop interior. The spatial derivatives are also central-differenced. The difference equations are arranged in a tridiagonal-matrix form, and a computationally inexpensive tridiagonal-matrix solver algorithm is employed. From known initial conditions, computations are made until the drop temperature approaches that of the far stream. A complete time–temperature history is developed in this manner.

6. Physical quantities of the problem

In this section equations are presented for obtaining the interfacial velocities, pressure profile, shear stress, drag, heat transfer, drop growth rate, and the bulk temperature of the drop. The dimensionless velocity components are

$$u_{g,\theta}|_{r=1} = u_\theta = \frac{1}{\sin\theta}\frac{\partial \psi_g}{\partial r}\bigg|_{r=1}, \tag{16a}$$

$$u_{g,r}|_{r=1} = \hat{u}_c = \frac{u_c}{Pe_{g,m}} = -\frac{1}{\sin\theta}\frac{\partial \psi_g}{\partial \theta}\bigg|_{r=1}. \tag{16b}$$

In order to obtain the pressure profile, consider the momentum equation

$$\nabla(v^2 + p_g) = 2\boldsymbol{u}_g \times \boldsymbol{\zeta}_g - \frac{4}{Re_g}\nabla \times \boldsymbol{\zeta}_g, \tag{17}$$

where

$$v^2 = u_{g,\theta}^2 + u_{g,r}^2.$$

The gas-phase stagnation pressure $p_{g,0}$ is obtained by an integration of the r-component of (17) along $\theta = 0$:

$$p_{g,0} = 1 + \frac{8}{Re_g}\int_1^{R_\infty} \frac{1}{r}\frac{\partial \zeta_g}{\partial \theta}\bigg|_{\theta=0} \mathrm{d}r - \hat{u}_c^2|_{\theta=0}. \tag{18}$$

The surface-pressure profile $p_{g,s}$ can be evaluated by integrating the θ-component of (17) along the interface:

$$p_{g,s} = p_{g,0} + \hat{u}_c^2|_{\theta=0} - (\hat{u}_c^2 + u_\theta^2) + \int_0^\theta \left[-2\hat{u}_c\zeta_g + \frac{4}{Re_g}\left\{\zeta_g + \frac{\partial \zeta_g}{\partial r}\right\}\right]_{r=1} \mathrm{d}\theta. \tag{19}$$

The dimensionless surface shear stress σ, scaled by $\mu_g U_\infty/R$, is

$$\begin{aligned}\sigma &= \left[r\frac{\partial}{\partial r}\left(\frac{u_{g,\theta}}{r}\right) + \frac{1}{r}\frac{\partial u_{g,r}}{\partial \theta}\right]\bigg|_{r=1} \\ &= \frac{1}{\sin\theta}\left\{\frac{\partial^2 \psi_g}{\partial r^2} - 2\frac{\partial \psi_g}{\partial r} - \frac{\partial^2 \psi_g}{\partial \theta^2} + \cot\theta\frac{\partial \psi_g}{\partial \theta}\right\}\bigg|_{r=1}.\end{aligned} \tag{20}$$

The pressure-drag, friction-drag and condensation-drag coefficients are

$$D_p = \int_0^\pi p_{g,s}\sin 2\theta \,\mathrm{d}\theta, \tag{21a}$$

$$D_f = \frac{8}{Re_g}\int_0^\pi \left\{\sigma\sin\theta - 2\frac{\partial u_{g,r}}{\partial r}\bigg|_{r=1}\cos\theta\right\}\sin\theta\,\mathrm{d}\theta, \tag{21b}$$

$$D_c = 4\int_0^\pi [\hat{u}_c\cos\theta - u_\theta\sin\theta]\,\hat{u}_c\sin\theta\,\mathrm{d}\theta. \tag{21c}$$

The condensation drag arises owing to the momentum associated with the radial flow. The total-drag coefficient

$$D_t = D_p + D_f + D_c. \tag{21d}$$

The average condensation velocity $\bar{u}_c$ and the average heat flux $\bar{q}$ at the drop surface are obtained as

$$\bar{u}_c = \frac{1}{2}\int_0^\pi u_c\sin\theta\,\mathrm{d}\theta, \qquad \bar{q} = \frac{1}{2}\int_0^\pi q\sin\theta\,\mathrm{d}\theta. \tag{22), (23}$$

For later reference, an expression for the non-dimensional condensation velocity $u_{c,0}$ for a stagnant drop is also presented. This is

$$u_{c,0} = 2\ln(1-W). \tag{24}$$

The derivation of $u_{c,0}$ in terms of W is given in Appendix B. The dimensionless growth rate for the drop is given by

$$\frac{1}{\bar{R}}\frac{d\bar{R}}{dt} = -\frac{D_{12}}{2\alpha_\ell}\frac{\rho_g}{\rho_\ell}\bar{u}_c. \tag{25}$$

The rate of change of the drop bulk temperature may be shown to be

$$\frac{dT_b}{dt} = -16\left.\frac{\partial \bar{T}_\ell}{\partial m}\right|_0, \tag{26}$$

where $T_b = (1/v)\int T_\ell \, dv$ and v is drop volume.

7. Results and discussion

The quasi-steady hydrodynamic and heat-transfer results are presented for various combinations of Re_g and W. Transient results for the drop heat-up and the growth rate are also presented for prescribed initial conditions. The numerical predictions have been compared with experimental results where available.

Figure 3 is a plot of the ratio $\bar{u}_c/u_{c,0}$ for various of Re_g and W. This graph depicts two features: (*a*) the enhancement in condensation rate due to drop translation; and (*b*) the role played by the condensation parameter W. For small values of W (large $m_{1,\infty}$ and/or a small thermal driving force $\Delta T = T_\infty - T_s$), the radial velocity induced by condensation is small. In such circumstances, the mass-transfer resistance to condensation offered by the non-condensable is essentially controlled by the translational flow field characterized by Re_g. The enhancement in condensation rate becomes mainly a function of Re_g. In the figure this feature is noted for $W = 0.1$ and 0.3. The graph also shows an excellent comparison between our numerical results and an experimental correlation applicable for low-W situations (Frössling 1938; Semian 1956; Kulic *et al.* 1975). For condensation on a moving drop $\bar{u}_c$ may be predicted by $\bar{u}_c/u_{c,0} = 1 + 0.276 Re_g^{\frac{1}{2}} Sc^{\frac{1}{3}}$. The solid line in the figure corresponds to this experimental correlation. For high values of W the effect of the radial flow on transport becomes significant. For $Re_g = O(100)$ the numerical results predict a relationship of the form $\bar{u}_c/u_{c,0} - 1 \propto Re_g^{\frac{1}{2}}$. Since $\bar{u}_c$ depends directly on the average concentration gradient of the non-condensable at the interface, this square-root dependence may be attributed to a boundary-layer-type variation for the non-condensable concentration.

Figure 4 shows the variation of the condensation velocity u_c with angle θ at a fixed W. At the front stagnation point, where the concentration gradient is the steepest, u_c is maximum. With increasing angle, u_c decreases up to the separation ring and varies approximately as $\cos\theta$. Near the separation ring u_c approaches $u_{c,0}$ independently of Re_g. The effect of translation on condensation is least felt at the separation ring in view of the small local velocity. Beyond the separation ring, in the rear of the drop, u_c increases with angle. This is due to the recirculation in the wake. With higher Re_g the strength of recirculation is higher and the enhancement in u_c is also larger.

The variation in surface shear stress σ with Re_g and W is plotted in figure 5. In the front portion of the drop the stress σ increases with Re_g and also with W. However, in the rear σ has opposite dependence on Re_g and W. These features may be

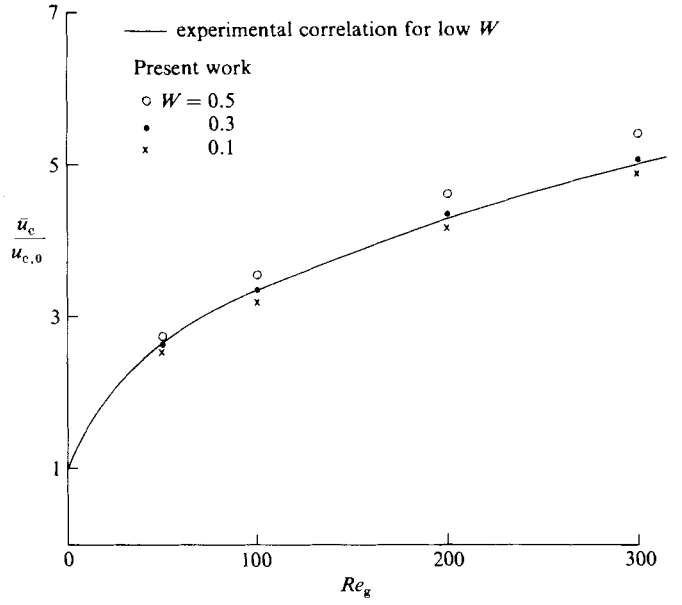

FIGURE 3. The variation of $\bar{u}_c/u_{c,0}$ with Re_g and W. Comparison between numerical results and experimental correlation.

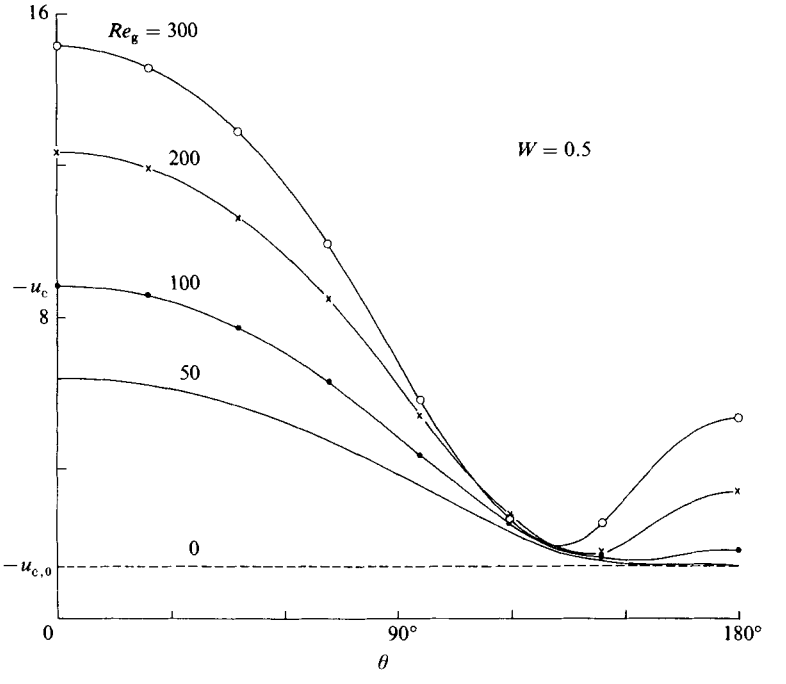

FIGURE 4. The variation of condensation velocity u_c with θ and Re_g.

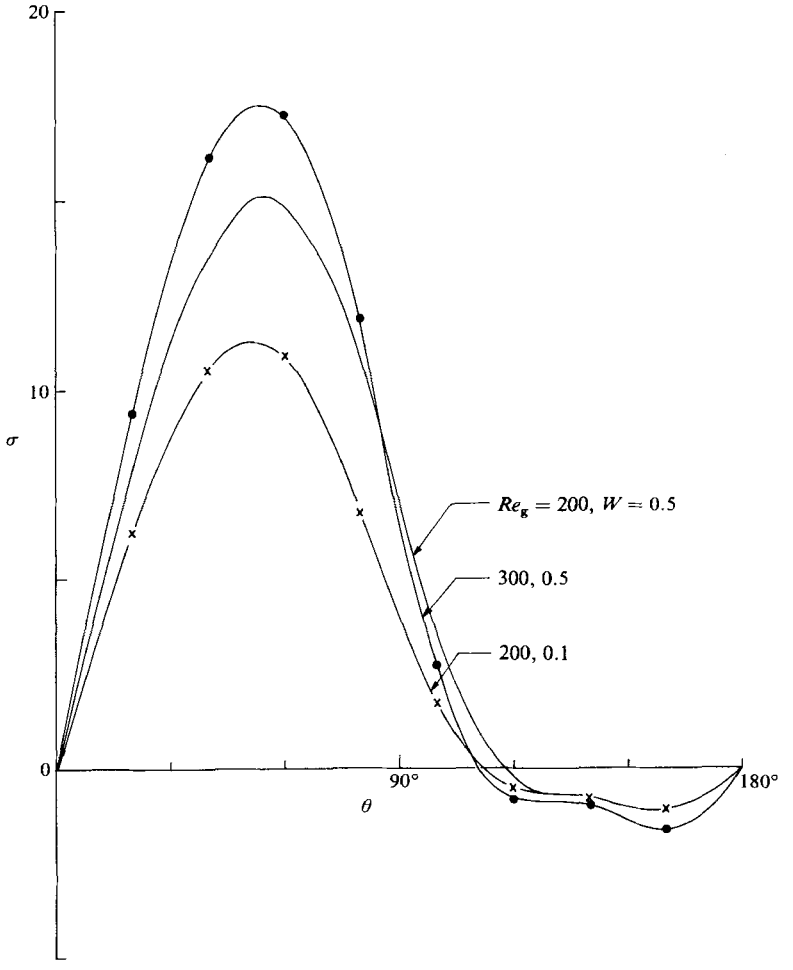

FIGURE 5. The variation in surface shear stress σ with θ, Re_g and W.

understood by envisioning a thin boundary-layer region of steep gradients in the front portion of the drop and a wake with weak gradients at the rear. The momentum boundary layer is thin at high Re_g or W (note that condensation is like suction). As a result, the radial gradient of the tangential velocity is higher and there is an increase in shear stress (equation (20)). At the rear of the drop, the magnitude of the negative shear stress is determined by the strength of the wake recirculation. At a high Re_g the viscous diffusion of momentum away from the drop surface is higher, and the flow separates earlier. The wake volume is increased, the strength of recirculation is larger, and the magnitude of the shear stress is higher. In contrast, at a high W, the radially inward convective transport of momentum is higher. There is greater availability of momentum in the flow direction. The angular extent of the wake is decreased, the strength of recirculation is reduced, and the magnitude of the shear stress decreases.

In figure 6 the dimensionless surface tangential velocity u_θ is plotted against θ, for various Re_g and W. The tangential velocity varies approximately as $\sin\theta$ (note that, in the Hill's vortex solution also, $u_\theta \propto \sin\theta$). By examining the curves for $Re_g = 200$, $W = 0$ and $Re_g = 200$, $W = 0.5$ it is clear that condensation inhibits the

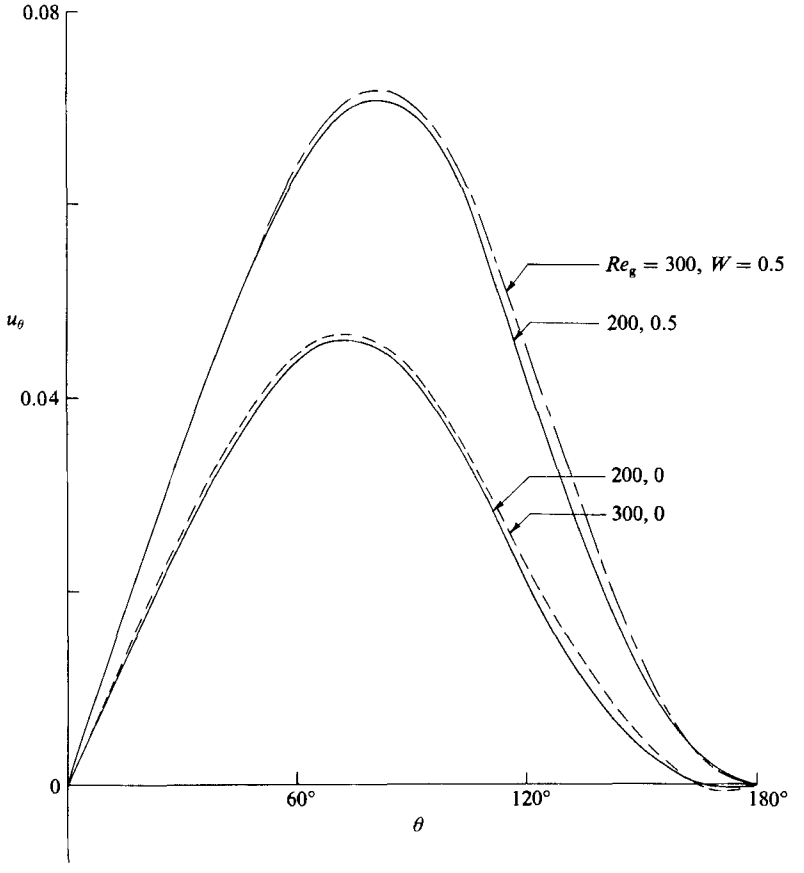

FIGURE 6. The variation of surface tangential velocity u_θ with θ, Re_g and W.

appearance of the secondary internal vortex motion in the drop. This is because, with higher W, the negative shear stress in the rear of the drop decreases in magnitude, while the forward shear increases. At a fixed W the strengths of both the primary and the secondary internal vortices increase with Re_g. Also, in the range of Reynolds numbers investigated here, the size of the secondary internal eddy increases with Re_g. Furthermore, for fixed W, u_θ increases with Re_g, but approaches a limiting profile. A similar trend has been noted in the absence of condensation by LeClair *et al.* (1972).

The gaseous-phase pressure profile at the drop surface changes drastically with condensation (figure 7). For flow around liquid spheres, in the absence of condensation, there is very little pressure recovery in the rear (Clift *et al.* 1978). With condensation there is a large pressure recovery. With $\hat{u}_c = O(Re_g^{-\frac{1}{2}})$, $\zeta_g = O(Re_g^{\frac{1}{2}})$ and $u_\theta = O(10^{-1})$, from (19), it is clear that the pressure profile is predominantly determined from a balance between the diffusive and the convective transports of vorticity. For $\hat{u}_c = 0$ (no condensation) the diffusion of vorticity away from the drop causes pressure loss in the rear. With condensation the radially inward flow counters this outward diffusion of vorticity. There is a wavy bump in the pressure profile at the rear. This is due to the enhancement in condensation velocity caused by wake recirculation. The pressure variations with Re_g (at constant W) suggest that at higher Re_g the convection of vorticity is more effective compared to diffusion.

The effects of condensation on the external and internal flow patterns are examined

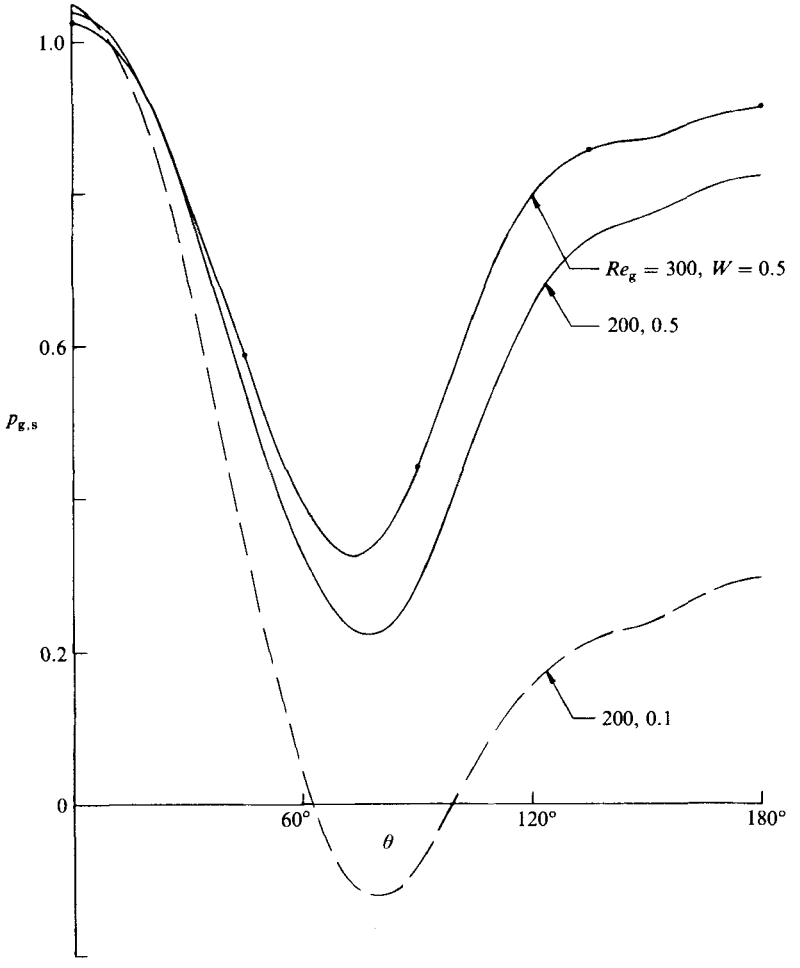

FIGURE 7. Effect of condensation on the pressure profile.

in figures 8 and 9. The situations $W = 0.1$ and 0.7, corresponding to low and high condensation rates, are depicted. The external flow pattern has a dividing stream surface (b or b') that intersects the rear axis at right angles. This point of intersection is truly a stagnation point with $\boldsymbol{u}_g = 0$. At low rates of condensation the dividing stream surface separates the recirculating region from the forward flow. All the fluid particles that are enclosed between the dividing stream surface and the drop surface either condense at the interface or recirculate in the wake region. Flow separation and recirculation in the wake are completely suppressed at a high level of condensation. The circulation-vortex strength (figure 9) increases with condensation owing to increased shear stress. The primary vortex centre shifts towards the drop equatorial plane as W is increased. The reduction in wake volume leads to greater fore-and-aft symmetry in the shear-stress profile at the drop surface; there is a corresponding reduction in the asymmetry in the circulation itself. Independently of the shear-stress profile, at high Re_ℓ, the circulation pattern resembles a Hill's vortex owing to increased advection of vorticity.

From figures 10 and 11 the coefficients for the friction drag D_f and the condensation drag D_c are noted to increase with W, while the pressure-drag coefficient D_p decreases

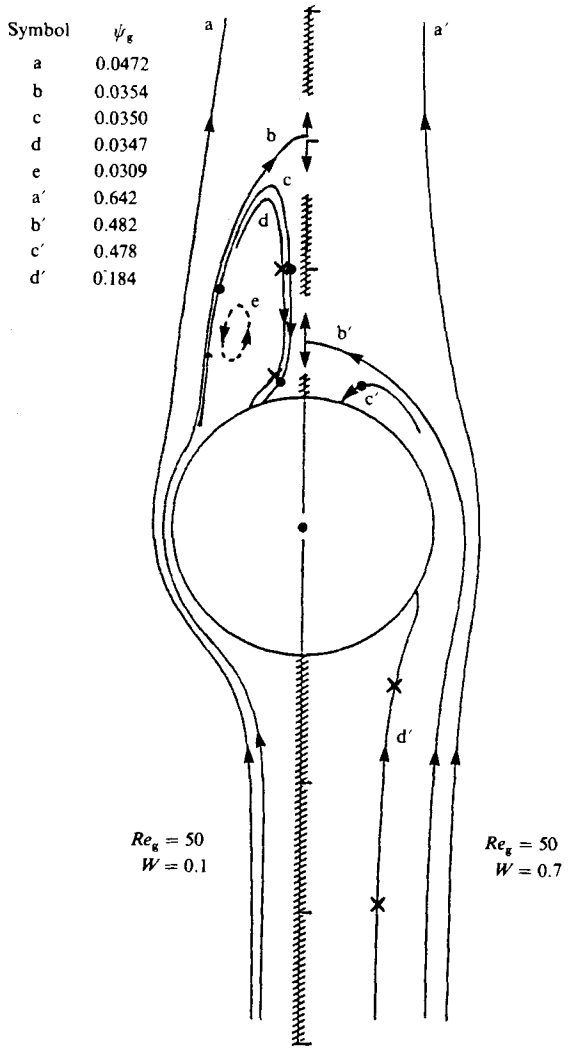

FIGURE 8. The effect of condensation on the external flow pattern (stream-function values are shown in key).

rapidly. D_f increases owing to the increase in shear stress, and D_c, which arises owing to the momentum of the radial flow, also increases. The decrease in D_p is due to the large pressure gain in the rear. The pressure-drag variation becomes important at larger Re_g or W, while the D_f variation is important at lower values. The condensation drag needs consideration at lower Re_g or high W. The variations in D_f and D_p profoundly influence D_t. At higher Re_g (figure 10), D_t decreases monotonically with W. However, at lower Re_g, D_t first increases but subsequently decreases with W (figure 11). Some further details on the drag phenomena are included in Appendix C.

For a freely falling drop, a balance between drag and drop weight yields

$$D_t Re_g^2 = \frac{32}{3}\left[\frac{\rho_\ell}{\rho_g} - 1\right]\frac{g}{\nu_g^2} R^3. \tag{27}$$

The quantity $D_t Re_g^2$ is a measure of the drop size, and figure 12 is a plot of $(D_t Re_g^2)$ versus Re_g and W. Each curve of constant W (a combination of p_∞, T_∞ and T_s) has

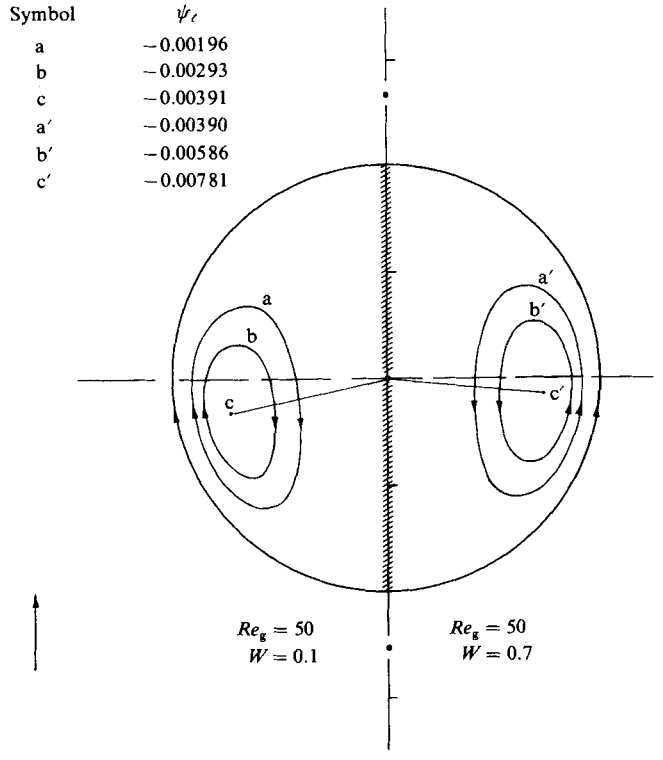

FIGURE 9. The effect of condensation on liquid circulation (stream-function values are shown in key).

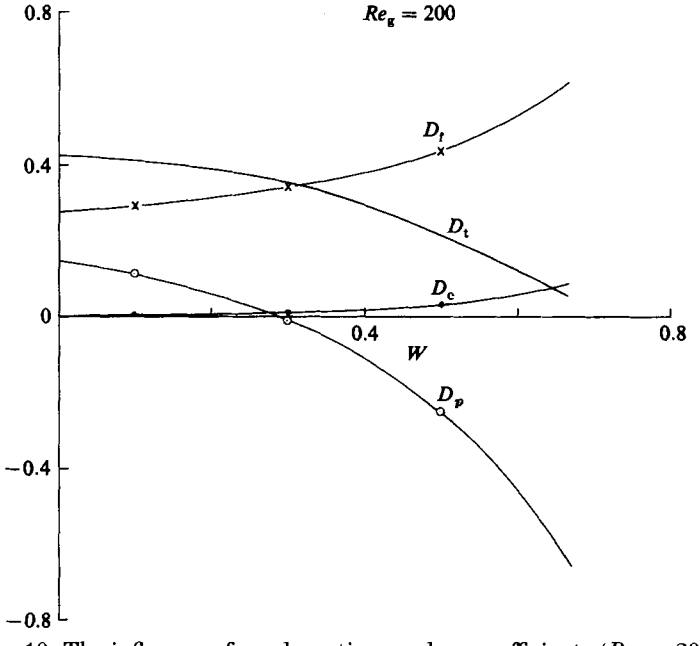

FIGURE 10. The influence of condensation on drag coefficients ($Re_g = 200$).

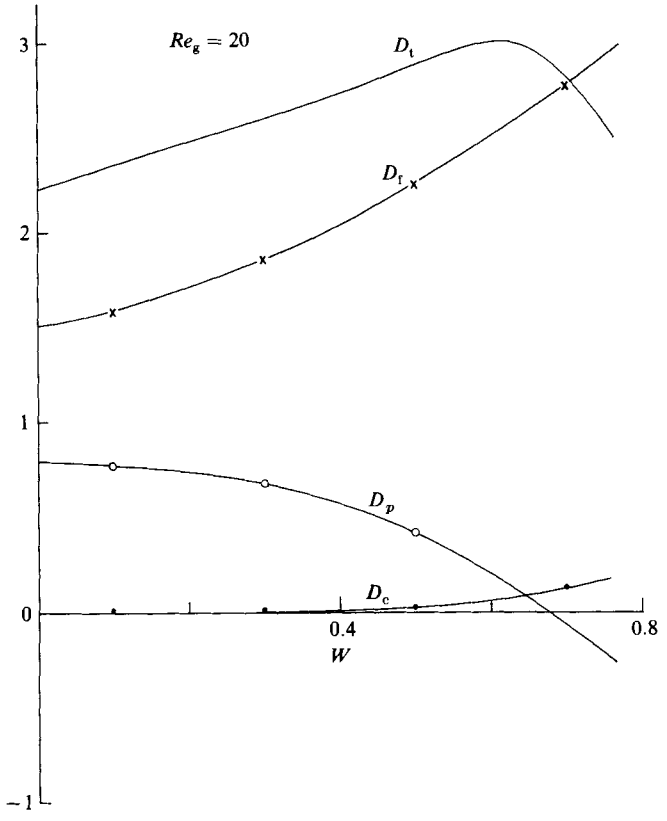

FIGURE 11. The influence of condensation on drag coefficients ($Re_g = 20$).

a maximum. This implies that there is a maximum drop size beyond which the drag force cannot balance the drop weight, and drops of a greater size would accelerate. For a given drop size, at each W, there are two possible motions corresponding to two different Re_g. But the values derived from the negative-slope parts of the curves correspond to unstable situations. It is the quasi-steady nature of the solution that provides the falling characteristic. For points on the negative-slope portion, as U_∞ increases, the corresponding drag is required to decrease. This is inadmissible. Also, as $W \to 0$, for points on the negative-slope portion $Re_g \to \infty$. Similar unstable solutions for rigid-sphere motion have been discussed by Clift *et al.* (1978).

In figure 13 the dimensionless average heat flux $\bar{q}$ to the drop is plotted against W and ΔT for various Re_g. The parameters p_∞ and T_∞ are given ($m_{1,\infty}$ is prescribed). We note that W has a maximum value $W_{max} = 1 - m_{1,\infty}$. The heat flux $\bar{q}$ increases in proportion to $\ln(1-W)$ and $Re_g^{\frac{1}{2}}$. This is analogous to $\bar{u}_c$, and the major contribution to the interfacial heat flux does, indeed, come from the latent heat of the condensing mass. A correlation for $\bar{u}_c$ can therefore be suitably interpreted for $\bar{q}$. For large ΔT, i.e. small T_s, the rate of increase of $\bar{q}$ with ΔT is small. This is because, for a given bulk concentration of the non-condensable, with increasing ΔT the interface non-condensable mass fraction increases steeply (Chung & Ayyaswamy 1978). The increased resistance to mass transfer causes a slower rate of increase in $\bar{q}$.

The variations of temperature inside the drop with distance from the drop surface and with time are shown in figure 14. The dimensionless liquid temperature $\bar{T}_\ell$, the

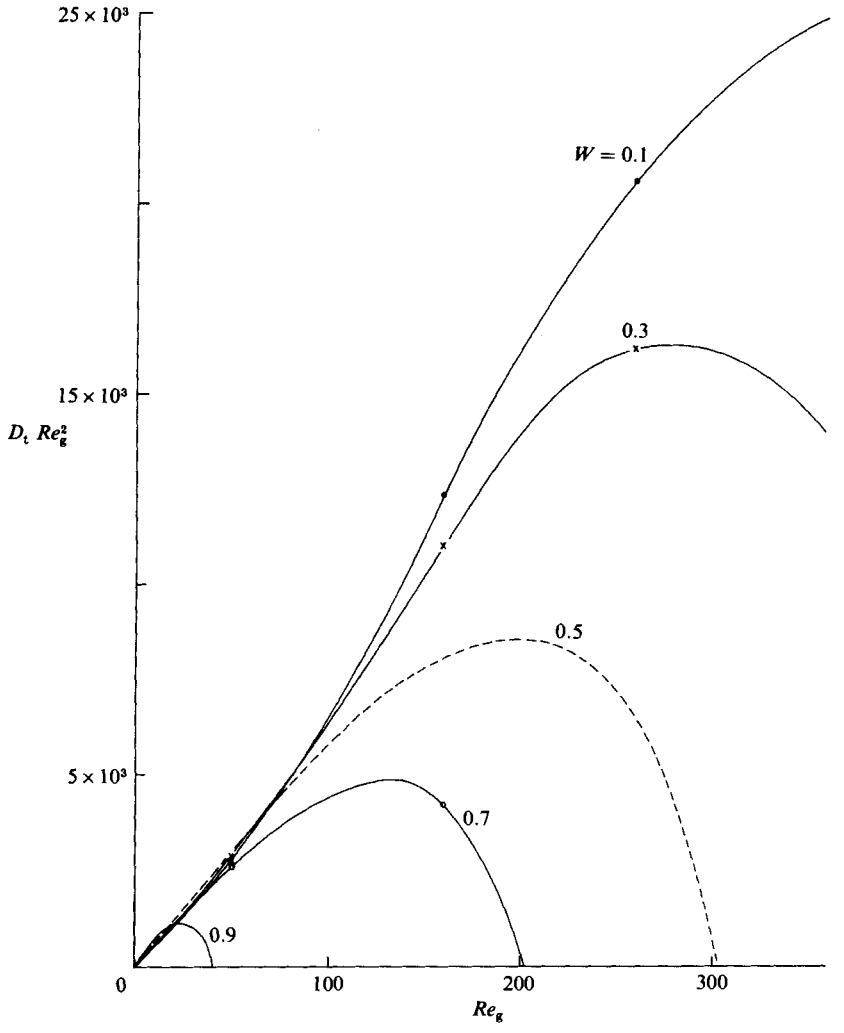

FIGURE 12. The relation between drop size, Re_g and W for a freely falling drop.

stream-function coordinate m and the dimensionless time t (thermal-diffusion timescale) characterize the description. For short times there is a steep increase in temperature across a thin layer of liquid that flows adjacent to the drop surface ($m = 0$). For large times the rate of increase of temperature in this layer is lower than that in the interior region. Most of the heat added at the surface of the drop is transferred to the drop core via diffusion across stream surfaces. This accounts for the higher rate of increase of the core temperature. For small times the form of the temperature profile depends upon the initial radius R_0 of the drop, and upon the drop initial temperature T_0. With increasing time the profile becomes similar (linear in m) for all starting conditions. A similar trend has been observed earlier by Brignell (1975) in a non-condensing situation. This implies that the bulk temperature T_b is a function of t only. From (12) and (26) it may be shown that, for large times, a 'developed' temperature

$$\hat{T} = T_b - 3H(m)\,\bar{T}_\ell = f(m)$$

describes the distribution. It is important to note that $\hat{T}$ is time-independent.

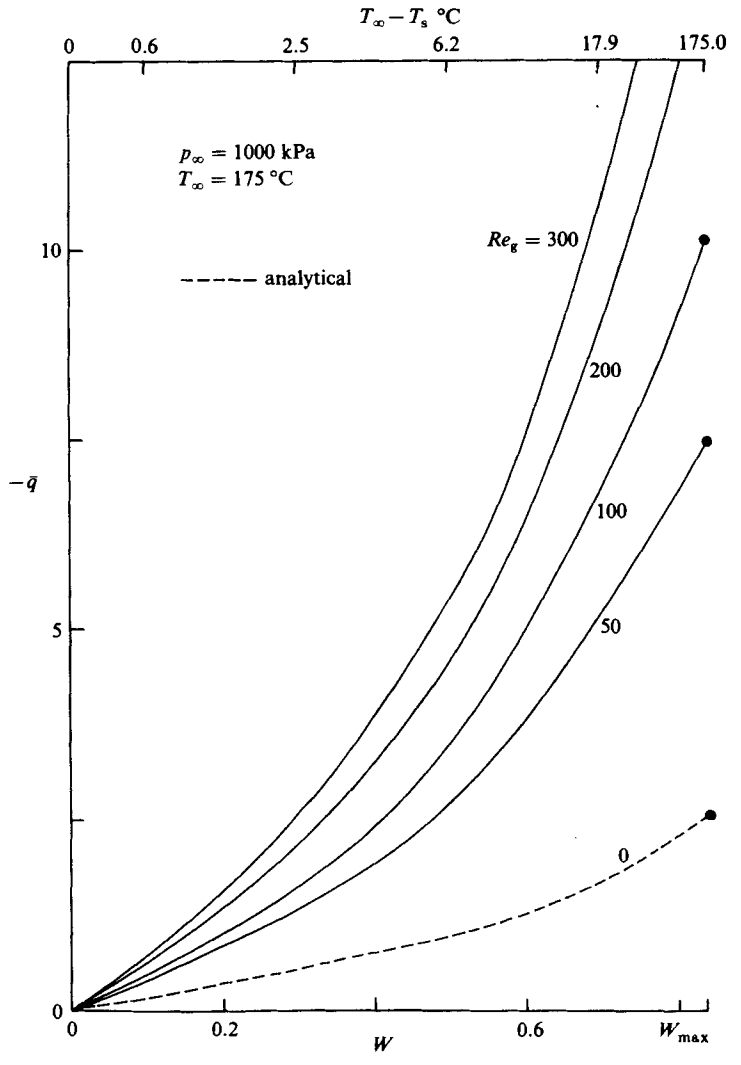

FIGURE 13. The variation in average heat flux with Re_g, W and ΔT.

The rate of drop growth is examined in figure 15 through a plot of the dimensionless radius $\bar{R}$ with t. The growth rate increases linearly with the temperature differential $\Delta T_0 = T_\infty - T_0$. By equating the total increase in enthalpy of the drop to the latent heat input through condensation, an approximate expression for the drop size $\bar{R}_f$ at the end of condensation results in the form

$$\bar{R}_f - 1 = \frac{C_{p\ell}\,\Delta T_0}{3\lambda}. \tag{28}$$

The results in figure 15 are in accordance with this expression. Since the drop growth rate is intimately connected with the drop heat-up rate, the variation of $\bar{R}$ with ΔT_0 and R_0 can be seen as a direct consequence of the manner in which the temperature profile inside the drop evolves in time.

Experimental measurements of the temperature–time history for a water drop experiencing condensation in a forced flow of air–steam mixture have been reported

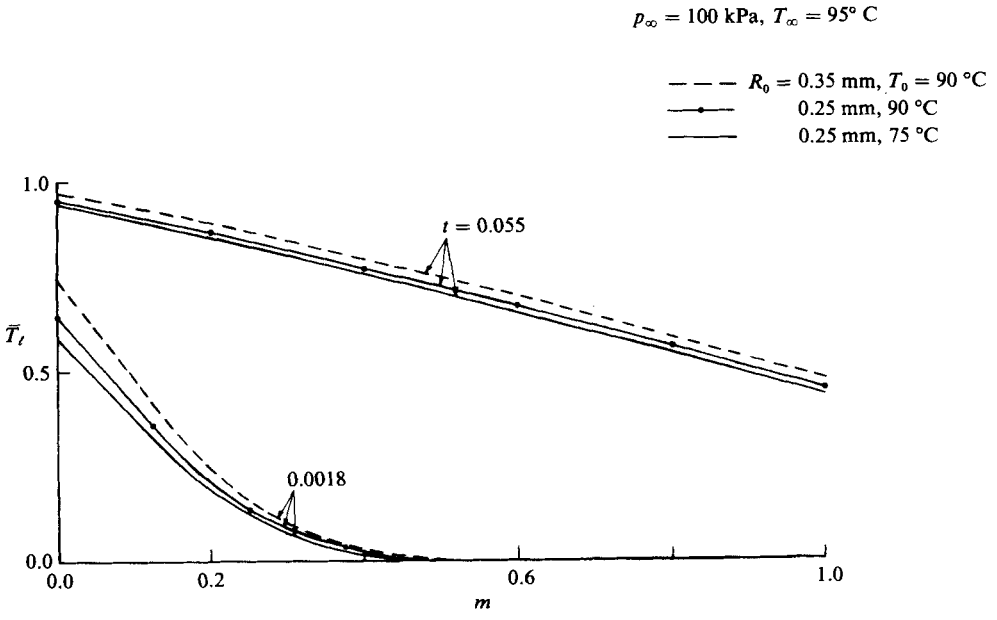

FIGURE 14. The temperature profile inside the drop.

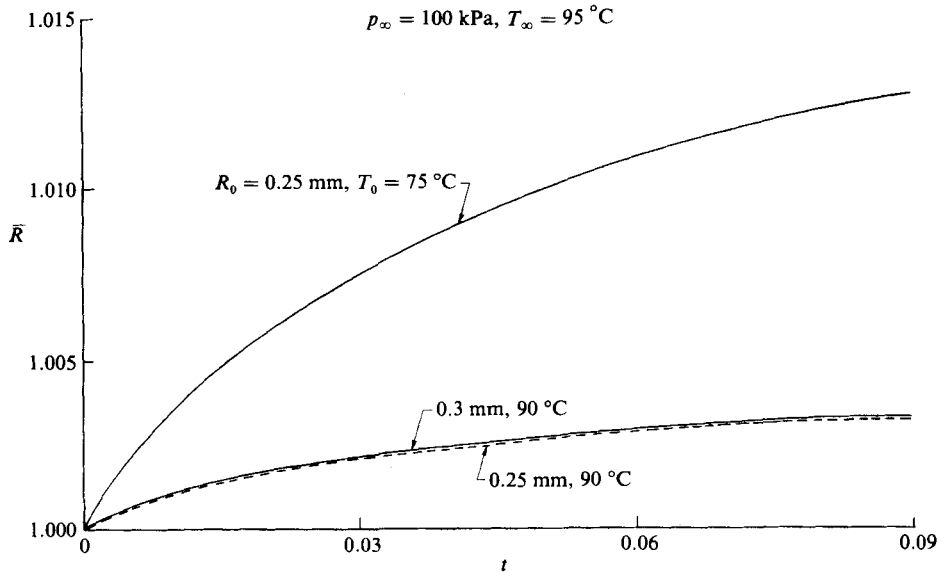

FIGURE 15. The drop growth rate.

by Kulic & Rhodes (1977). In figure 16 the comparisons between our numerical results and the experimental data are shown. The comparisons are for two situations: (i) $R_0 = 1.45$ mm, $U_\infty = 1.91$ m/s, $T_\infty = 80$ °C, $p_\infty = 1$ bar and $T_0 = 16$ °C ($Re_g \approx 265$); and (ii) $R_0 = 1.4$ mm, $U_\infty = 1.68$ m/s, $T_\infty = 72.5$ °C, $p_\infty = 1$ bar (or the far-stream volume fraction of steam $x_s = 35\,\%$) and $T_0 = 18$ °C ($Re_g \approx 225$). For the range of these parameters, the Eötvös number Eo is in excess of 0.4. In view of this, our analysis cannot be expected to provide accurate details of the fluid-flow characteristics.

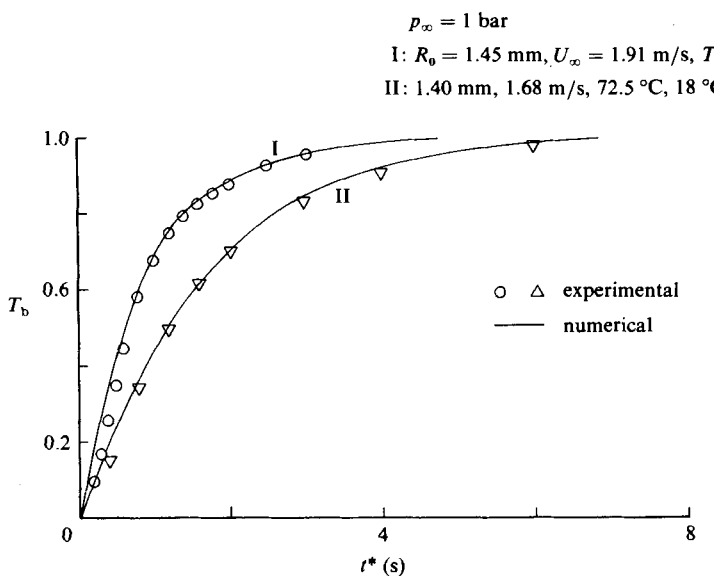

FIGURE 16. The variation of drop bulk temperature with time. Comparison of numerical results with experimental data.

However, the drop bulk temperatures (average quantities) are seen to be predicted excellently. The figure also shows that, for larger non-condensable fraction in the bulk, the drop heat-up rate is slower. This illustrates the effect of the gas-phase resistance.

The authors wish to acknowledge gratefully the many helpful discussions they have had with Professors E. B. Dussan V. and S. S. Sadhal (University of Southern California). Sponsorship of this work by the National Science Foundation grants MEA 80-23861 and MEA 82-17097 is also gratefully acknowledged.

Appendix A. Uniform-surface-temperature assumption

The surface temperature of a moving drop experiencing condensation in a vapour–gas atmosphere will never be uniform until the drop thermally equilibrates with the outside (condensation ceases). However, the parameter of interest to us is the ratio Ω of the angular variation in surface temperature T_s' to the average surface temperature $\bar{T}_s$. When Ω is small the assumption of a uniform surface temperature is reasonable and attractive.

During the initial transient period following drop introduction, the high condensation heat flux will raise the surface temperature rapidly. A moving fluid element near the drop surface will be heated continuously along its path and T_s' will be comparable to $\bar{T}_s$ ($\Omega = O(1)$). The time of this period is $O(R/U_s)$, or the time for a few internal circulation cycles. With an increased number of cycles, $\bar{T}_s$ increases, whereas T_s' actually decreases. By about ten circulation cycles (roughly one percent of the total condensation period for $Pe_\ell = O(10^3)$), Ω drops to a value $O(10^{-1})$, and the uniform-T_s assumption is justified for later periods. As the drop approaches thermal equilibrium with the outside, $\Omega \to 0$ and T_s becomes truly uniform.

For mathematical justification, consider an instantaneous surface heat flux of the form $q = \bar{q} + \hat{q}(\theta)$, where $\bar{q}$ is the average heat flux and $\hat{q}(\theta)$ is the angular variation.

Let q' be the maximum amplitude of $\hat{q}(\theta)$. Here $\bar{q}$ and q' may be of the same order ($q' \leqslant O(\bar{q})$). Applying heat-conduction theory appropriate for small times (treating the drop as semi-infinite in the radial direction), we estimate the maximum variation in surface temperature T'_s, and the increase $\Delta\bar{T}_s$ in average temperature per circulation cycle as

$$T'_s = O\left(\frac{(\bar{q}+q')\,R\,Pe_\ell^{-\frac{1}{2}}}{k_\ell}\right),$$

$$\Delta\bar{T}_s \sim O\left(\frac{\bar{q}R\,Pe_\ell^{-\frac{1}{2}}}{k_\ell}\right),$$

where k_ℓ is the liquid thermal conductivity. Therefore, for the first circulation cycle the ratio Ω is seen to be

$$\Omega = O\left(\frac{\bar{q}+q'}{\bar{q}}\right) = O(1).$$

However, $\bar{T}_s$ increases with each cycle, and in fact $\bar{T}_s = \Sigma_{i-1}^{N} \Delta\bar{T}_{s,i}$, where N is the number of circulation cycles, and $\Delta\bar{T}_{s,i}$ is the increment for the ith cycle. On the other hand, T'_s remains of the same order for all N, since all the fluid particles on a stream surface are exposed to the same heating conditions, over a complete circulation cycle. Hence, as before,

$$T'_s = O\left(\frac{(\bar{q}+q')\,R\,Pe_\ell^{-\frac{1}{2}}}{k_\ell}\right) \quad \text{for all } N.$$

Since $\bar{q}$ and q' decrease with each circulation cycle, a general expression for Ω is given by

$$\Omega = O\left(\frac{\bar{q}_N + q'_N}{\sum_{i=1}^{N} \bar{q}_i}\right).$$

Thus it follows that $\Omega \to 0$ as $N \to \infty$.

Appendix B. Spherically symmetric condensation

Consider a stationary drop experiencing spherically symmetric condensation in the presence of a non-condensable. The continuity and species transport equations are

$$\frac{1}{r^2}\frac{\partial}{\partial r}(r^2 u_{g,r}) = 0 \quad \text{(continuity)}, \tag{B 1}$$

$$u_{g,r}\frac{\partial w_1}{\partial r} = \frac{2}{r^2}\frac{\partial}{\partial r}\left(r^2\frac{\partial w_1}{\partial r}\right) \quad \text{(species)}, \tag{B 2}$$

where $u_{g,r}$ has been scaled by $D_{12}/2R$. From (B 1) we get

$$u_{g,r} = u_{c,0}/r^2, \tag{B 3}$$

where $u_{c,0}$ is the condensation velocity (at $r = 1$). The boundary conditions on w_1 are

$$w_1 = 1 \quad \text{at } r = 1, \quad w_1 = 0 \quad \text{as } r \to \infty. \tag{B 4}$$

Solving (B 2) subject to (B 4),

$$w_1 = \left[1 - \exp\left\{-\frac{u_{c,0}}{2r}\right\}\right] \Big/ \left[1 - \exp\{-\tfrac{1}{2}u_{c,0}\}\right]. \tag{B 5}$$

The condensation velocity $u_{c,0}$ is determined from the impermeability condition for the non-condensable at the interface, viz

$$2W\frac{\partial w_1}{\partial r}\bigg|_{r=1} = u_{c,0}. \tag{B 6}$$

Using (B 5) in (B 6),

$$u_{c,0} = 2\ln(1-W). \tag{B 7}$$

Appendix C. A correlation for drag on the drop

Noting that $\bar{u}_c \propto \ln(1-W)$, from the continuity equation (1), we can estimate

$$u_\theta \propto \ln(1-W), \quad \frac{\partial u_\theta}{\partial r} \propto \ln(1-W).$$

Using these estimates in (19)–(21), it may be inferred that D_c and D_p have an approximately parabolic dependence on $\ln(1-W)$, and D_f has an approximately linear dependence on the same factor. Also, a careful examination of (21*a–c*) reveals that D_p is $O(1)$, D_f is $O(Re_g^{-\frac{1}{2}})$ and D_c is $O(Re_g^{-1})$. A correlation for the total-drag coefficient D_t may be obtained in the form

$$D_t = f_1(y)\,x^2 + f_2(y)\,x + f_3(y), \tag{C 1}$$

where

$$y = Re_g^{-\frac{1}{2}}, \quad x = \ln(1-W),$$

$$f_1(y) = 11303y^3 - 3304.6y^2 + 300.37y - 8.8029,$$

$$f_2(y) = 8890.1y^3 - 2598.2y^2 + 228.73y - 6.0811,$$

$$f_3(y) = 2559.5y^3 - 731.69y^2 + 74.335y - 2.0658.$$

The above correlation predicts the drag coefficient within 1% of the numerically computed values in the Reynolds-number range 30–300 and condensation-parameter range 0–0.9. The property ratios are $\mu_\ell/\mu_g \approx 40$ and $\rho_\ell/\rho_g \approx 1000$.

REFERENCES

Batchelor, G. K. 1956 On steady laminar flow with closed streamlines at large Reynolds number. *J. Fluid Mech.* **1**, 177–190.

Brignell, A. S. 1975 Solute extraction from an internally circulating spherical liquid drop. *Intl J. Heat Mass Transfer* **18**, 61–68.

Chung, J. N. & Ayyaswamy, P. S. 1978 Laminar condensation heat and mass transfer in the vicinity of the forward stagnation point of a spherical droplet translating in a ternary mixture: numerical and asymptotic solutions. *Intl J. Heat Mass Transfer* **21**, 1309–1324.

Chung, J. N. & Ayyaswamy, P. S. 1981*a* Laminar condensation heat and mass transfer to a moving drop. *AIChE J.* **27**, 372–377.

Chung, J. N. & Ayyaswamy, P. S. 1981*b* Material removal associated with condensation on a droplet in motion. *Intl J. Multiphase Flow* **7**, 329–342.

Chung, J. N., Ayyaswamy, P. S. & Sadhal, S. S. 1984*a* Laminar condensation on a moving drop. Part 1. Singular perturbation technique. *J. Fluid Mech.* **139**, 105–130.

Chung, J. N., Ayyaswamy, P. S. & Sadhal S. S. 1984*b* Laminar condensation on a moving drop. Part 2. Numerical solutions. *J. Fluid Mech.* **139**, 131–144.

Clift, R., Grace, J. R. & Weber, M. E. 1978 *Bubbles, Drops and Particles.* Academic.

Ford, J. D. & Lekic, A. 1973 Rate of growth of drops during condensation. *Intl J. Heat Mass Transfer* **16**, 61–64.

Frössling, N. 1938 Über die Verdunstung fallenden Tropfen. *Gerlands Beitr. Geophys.* **52**, 170–216.

GUPTA, M. M. 1973 A discussion of papers by D. B. Spalding and A. K. Runchal. *J. Numer. Meths Engng* **4**, 560–563.

HARPOLE, G. M. 1981 Droplet evaporation in high temperature environments. *Trans. ASME* C: *J. Heat Transfer* **103**, 86–91.

JOSEPH, M. 1983 Finite difference representations of vorticity transport. *Comp. Meths Appl. Mech. Engng* **39**, 107–116.

KRONIG, R. & BRINK, J. C. 1950 On the theory of extraction from falling droplets. *Appl. Sci. Res.* A **2**, 142–154.

KULIC, E. & RHODES, E. 1977 Direct contact condensation from air–steam mixtures on a single droplet. *Can. J. Chem. Engng* **55**, 131–137.

KULIC, E. & RHODES, E. 1978 Heat transfer rates to moving droplets in air/steam mixtures. In *Proc. 6th Intl Heat Transfer Conf., Toronto*, pp. 464–474.

KULIC, E., RHODES, E. & SULLIVAN, G. 1975 Heat transfer rate predictions in condensation on droplets from air–steam mixtures. *Can. J. Chem. Engng* **53**, 252–258.

LAW, C. K., PRAKASH, S. & SIRIGNANO, W. A. 1977 Theory of convective, transient, multi component droplet vaporization. In *Proc. 16th Symp. (Intl) on Combustion*, pp. 605–617. The Combustion Institute.

LECLAIR, B. P., HAMIELEC, A. E., PRUPPACHER, H. R. & HALL, W. D. 1972 A theoretical and experimental study of the internal circulation in water drops falling at terminal velocity in air. *J. Atmos. Sci.* **29**, 728–740.

LOU, Y. S. & YANG, L. S. 1978 Quasi-steady theory of non-equilibrium droplet evaporation and condensation. *J. Appl. Phys.* **50**, 5331–5338.

NIX, N. & FUKUTA, N. 1972 Nonsteady-state theory of droplet growth. *J. Chem. Phys.* **58**, 1735–1740.

PATANKAR, S. V. 1980 *Numerical Heat Transfer and Fluid Flow*. McGraw-Hill, New York.

RAITHBY, G. D. 1976 A critical evaluation of upwind differencing applied to problems involving fluid flow. *Comp. Meths Appl. Mech. Engng* **9**, 153–164.

RAKHMATULINA, I. KH. 1981 Nonsteady evaporation and growth of drops in gas(eous) medium. *Intl J. Engng Sci.* **19**, 1114–1122.

RUNCHAL, A. K. 1972 Convergence and accuracy of three finite difference schemes for a two-dimensional conduction and convection problem. *Intl J. Numer. Meths Engng* **4**, 541–550.

SADHAL, S. S. & AYYASWAMY, P. S. 1983 Flow past a liquid drop with a large non-uniform radial velocity. *J. Fluid Mech.* **133**, 65–81.

SEMIAN, V. M. 1956 Heat transfer from wet air by vapour condensation. *Teploenergetica* **4**.

SPALDING, D. B. 1972 A novel finite difference formulation for differential equations involving both first and second derivatives. *Intl J. Numer. Meths Engng* **7**, 551–559.

STRIKWERDA, J. C. 1982 Upwind differencing, false scaling and non-physical solutions to the driven cavity problem. *J. Comp. Phys.* **47**, 303–307.

SUNDARARAJAN, T. & AYYASWAMY, P. S. 1984*a* Heat and mass transfer associated with condensation on a moving drop: Solutions for intermediate Reynolds numbers by a boundary layer formulation. *Trans. ASME* C: *J. Heat Transfer* (in press).

SUNDARARAJAN, T. & AYYASWAMY, P. S. 1984*b* Condensation on a moving drop: transient evolution of the drop interior. Submitted for publication.

VAHL DAVIS, G. DE & MALLINSON, G. D. 1976 An evaluation of upwind and central difference approximations by a study of recirculating flow. *Comp. Fluids* **4**, 29–43.